LETTER

doi:10.1038/nature14602

Nanotubes mediate niche–stem-cell signalling in the *Drosophila* testis

Mayu Inaba[1,2,3], Michael Buszczak[3] & Yukiko M. Yamashita[1,2]

Stem cell niches provide resident stem cells with signals that specify their identity. Niche signals act over a short range such that only stem cells but not their differentiating progeny receive the self-renewing signals[1]. However, the cellular mechanisms that limit niche signalling to stem cells remain poorly understood. Here we show that the *Drosophila* male germline stem cells form previously unrecognized structures, microtubule-based nanotubes, which extend into the hub, a major niche component. Microtubule-based nanotubes are observed specifically within germline stem cell populations, and require intraflagellar transport proteins for their formation. The bone morphogenetic protein (BMP) receptor Tkv localizes to microtubule-based nanotubes. Perturbation of microtubule-based nanotubes compromises activation of Dpp signalling within germline stem cells, leading to germline stem cell loss. Moreover, Dpp ligand and Tkv receptor interaction is necessary and sufficient for microtubule-based nanotube formation. We propose that microtubule-based nanotubes provide a novel mechanism for selective receptor–ligand interaction, contributing to the short-range nature of niche–stem-cell signalling.

The *Drosophila* testis represents an excellent model system to study niche–stem-cell interactions because of its well-defined anatomy: eight to ten germline stem cells (GSCs) are attached to a cluster of somatic hub cells, which serve as a major component of the stem cell niche (Fig. 1a). The hub secretes at least two ligands: the cytokine-like ligand Unpaired (Upd), and a BMP ligand Decapentaplegic (Dpp), both of which regulate GSC maintenance[2–5]. GSCs typically divide asymmetrically, so that one daughter of the stem cell division remains attached to the hub and retains stem cell identity, while the other daughter, called a gonialblast, is displaced away from the hub and initiates differentiation[6]. Given the close proximity of GSCs and gonialblasts, the ligands (Upd and Dpp) must act over a short range so that signalling is only active in stem cells, but not in differentiating germ cells. The basis for this sharp boundary of pathway activation remains poorly understood.

Using green fluorescent protein (GFP)-α1-*tubulin84B* expressed in germ cells (*nos-gal4>UAS–GFP–αtub*), we found that GSCs form protrusions, referred to as microtubule-based (MT)-nanotubes hereafter, that extend into the hub (Fig. 1b). MT-nanotubes are sensitive to fixation similar to other thin protrusions reported so far, such as tunnelling nanotubes[7] and cytonemes[8], explaining why they have escaped detection in previous studies. MT-nanotubes appear to be specific to GSCs: we observed 6.67 MT-nanotubes per testis in the GSC population (or 0.82 per cell, $n = 73$ testes). The average thickness and length of MT-nanotubes are 0.43 ± 0.29 μm (at the base of MT-nanotube, $n = 51$ nanotubes) and 3.32 ± 1.6 μm ($n = 82$ nanotubes), respectively. These GSC MT-nanotubes are uniformly oriented towards the hub area (Fig. 1c). By contrast, differentiating germ cells

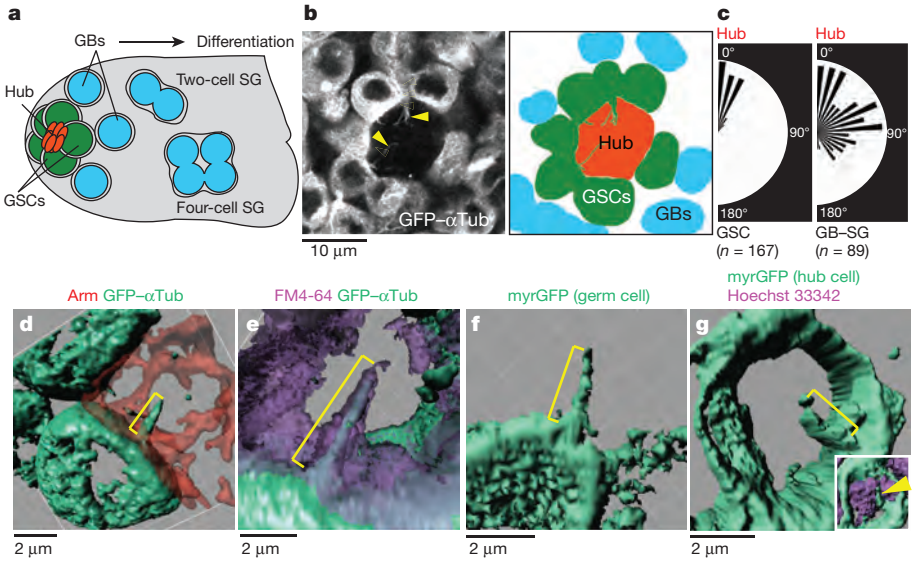

Figure 1 | Characterization of MT-nanotubes in *Drosophila* male GSC niche. **a**, Schematic of the *Drosophila* male GSC niche. GSCs are attached to the hub cells. The immediate daughters of GSCs, the gonialblasts (GBs) are displaced away from the hub, and become spermatogonia (SG). **b**, An apical tip of the testis expressing GFP–αTub in germ cells (*nos-gal4>GFP–αtub*). MT-nanotubes are indicated by arrowheads. A graphic interpretation is shown in the right-hand panel. **c**, Orientation of nanotubes towards the hub in GSCs versus gonialblasts/spermatogonia. The size of each vector represents the frequency of MT-nanotubes oriented towards each direction. Indicated numbers of nanotubes ($n > 30$ testes) were scored from three independent experiments. **d**–**g**, Three-dimensional rendering images of MT-nanotubes (brackets) in fixed (**d**) or live tissue (**e**–**g**), with indicated cell membrane markers; *nos-gal4>GFP–αtub* was used for **d** and **e**.

[1]Life Sciences Institute, Department of Cell and Developmental Biology Medical School, University of Michigan, Ann Arbor, Michigan 48109, USA. [2]Howard Hughes Medical Institute, University of Michigan Ann Arbor, Michigan 48109, USA. [3]Department of Molecular Biology, University of Texas Southwestern Medical Center at Dallas, Dallas, Texas 75390, USA.

showed only 0.44 MT-nanotubes per testis (or <0.002 per cell, $n = 75$ testes), without any particular orientation when present (Fig. 1c). MT-nanotubes were sensitive to colcemid, the microtubule-depolymerizing drug, but not to the actin polymerization inhibitor cytochalasin B, suggesting that MT-nanotubes are microtubule-based structures (Extended Data Fig. 1a–d, f). MT-nanotubes were not observed in mitotic GSCs (Extended Data Fig. 1e, g), and GSCs form new MT-nanotubes as they exit from mitosis (Extended Data Fig. 1h and Supplementary Video 1). By contrast, MT-nanotubes in interphase GSCs were stably maintained for up to 1 h of time-lapse live imaging (Supplementary Video 2). Although cell-cycle-dependent formation of MT-nanotube resembles that of primary cilia[9,10], MT-nanotubes are distinct structures, in that they lack acetylated microtubules and are sensitive to fixation. Furthermore, a considerable fraction of GSCs form multiple MT-nanotubes per cell (54% of GSCs with MT-nanotubes, $n = 251$ GSCs), and MT-nanotubes are not always associated with the centrosome/basal body, as is the case for the primary cilia (Extended Data Fig. 1i).

To examine the geometric relationship between MT-nanotubes and hub cells further, we imaged MT-nanotubes in combination with various cell membrane markers, followed by three-dimensional rendering. Although the MT-nanotubes are best visualized in unfixed testes that express GFP–αTub in germ cells, adding a low concentration (1 μM) of taxol to the fixative preserves MT-nanotubes, allowing immunofluorescence staining. First, Armadillo (Arm, β-catenin) staining, which marks adherens junctions formed at hub cell/hub cell as well as hub cell/GSC boundaries, revealed that adherens junctions do not form on the surface of MT-nanotubes (Fig. 1d and Supplementary Video 3). Using FM4-64 styryl dye, we found that the MT-nanotubes are ensheathed by membrane lipids (Fig. 1e and Supplementary Videos 4 and 5). Furthermore, myristoylation/palmitoylation site GFP (myrGFP), a membrane marker, expressed in either the germline (Fig. 1f) or hub cells (Fig. 1g) illuminated MT-nanotubes, suggesting that the surface membrane of a MT-nanotube is juxtaposed to hub-cell plasma membrane.

We examined genes that regulate primary cilia and cytonemes for their possible involvement in MT-nanotube formation (Fig. 2a). RNA interference (RNAi)-mediated knockdown of *oseg2* (*IFT172*), *osm6* (*IFT52*) and *che-13* (*IFT57*), components of the intraflagellar transport (IFT)-B complex that are required for primary cilium anterograde transport and assembly[11], significantly reduced the length and the frequency of MT-nanotubes (Fig. 2a, Extended Data Fig. 2b and Extended Data Table 1). Knockdown of *Dlic*, a dynein intermediate chain required for retrograde transport in primary cilia[12], also reduced the MT-nanotube length and frequency (Fig. 2a and Extended Data Table 1). Knockdown of *klp10A*, a *Drosophila* homologue of mammalian *kif24* (a MT-depolymerizing kinesin of the kinesin-13 family, which suppresses precocious cilia formation[13]), resulted in abnormally thick/bulged MT-nanotubes (Fig. 2a, Extended Data Fig. 2c and Extended Data Table 1). We did not observe significant changes in MT-nanotube morphology upon knockdown of IFT-A retrograde transport genes, such as *oseg1* and *oseg3* (Fig. 2a and Extended Data Table 1).

Endogenous Klp10A localized to MT-nanotubes both in wild-type testes and in GFP–αTub-expressing testes (Fig. 2b and Extended Data Fig. 2d, e). GFP–Oseg2 (IFT-B), GFP–Oseg1, GFP–Oseg3 (IFT-A) and Dlic also localized to the MT-nanotubes when expressed in germ cells (Fig. 2c and Extended Data Fig. 2f–i). The localization of IFT-A components to MT-nanotubes, without detectable morphological abnormality upon mutation/knockdown, is reminiscent of the observation that most of the genes for IFT-A are not required for primary cilia assembly[14–17]. Expression of a dominant negative form of Dia (Dia^{DN}) or a temperature-sensitive form of Shi (Shi^{ts}) in germ cells (*nos-gal4>UAS-dia*^{DN} or *UAS-shi*^{ts}), which perturb cytoneme formation[18], did not influence the morphology or frequency of MT-nanotubes in GSCs (Fig. 2a and Extended Data Table 1).

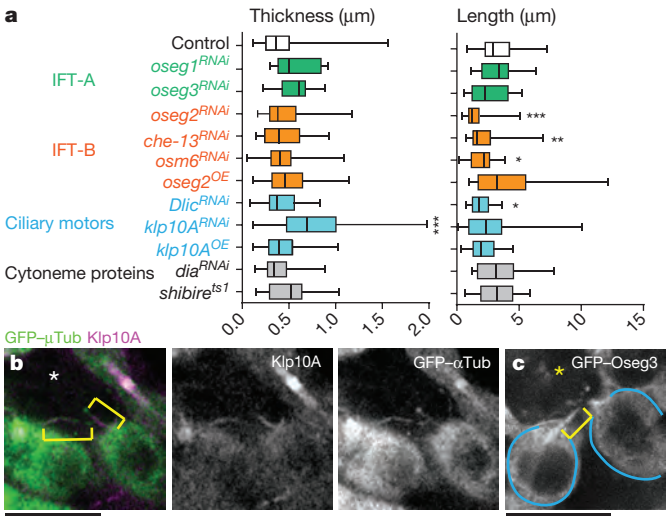

Figure 2 | IFT genes are required for MT-nanotube formation. **a**, Effect of RNAi-mediated knockdown or overexpression (OE) of indicated genes on MT-nanotube morphology. Box plot shows 25–75% (box), median (band inside) and minima to maxima (whiskers). Indicated numbers of MT-nanotubes (Extended Data Table 1) from at least two independent crosses were scored for each data point. *P* values from *t*-tests are provided as $*P \leq 0.05$, $**P \leq 0.01$ and $***P \leq 0.001$. **b**, Examples of MT-nanotubes stained by anti-Klp10A antibody in GFP–αTub-expressing testis. **c**, Apical testis tip expressing GFP–Oseg3 in germ cells. MT-nanotube is indicated by brackets. GSCs are indicated by blue lines. Asterisk indicates hub. Scale bar, 10 μm.

Taken together, these results show that primary cilia proteins localize to MT-nanotubes and regulate their formation.

In search of the possible involvement of MT-nanotubes in hub–GSC signalling, we found that the Dpp receptor, Thickveins (Tkv), expressed in germ cells (*nos-gal4>tkv–GFP*) was observed within the hub region (Extended Data Fig. 3a), in contrast to GFP alone, which remained within the germ cells (Extended Data Fig. 3b). A GFP protein trap of Tkv (in which GFP tags Tkv at the endogenous locus) also showed the same localization pattern as Tkv–GFP expressed by *nos-gal4* (Extended Data Fig. 3c). By inducing GSC clones that co-express Tkv–mCherry and GFP–αTub, we found that Tkv–mCherry localizes along the MT-nanotubes as puncta (Fig. 3a). Furthermore, using live observation, Tkv–mCherry puncta were observed to move along the MT-nanotubes marked with GFP–αTub (Extended Data Fig. 3d), suggesting that Tkv is transported towards the hub along the MT-nanotubes. It should be noted that, in the course of our study, we noticed that mCherry itself localized to the hub when expressed in germ cells, similar to Tkv–GFP and Tkv–mCherry (see Extended Data Fig. 3e, f and Supplementary Note 1). Importantly, the receptor for Upd, Domeless (Dome), predominantly stayed in the cell body of GSCs (Extended Data Fig. 3g), demonstrating the specificity/selectivity of MT-nanotubes in trafficking specific components of the niche signalling pathways. A reporter of ligand-bound Tkv, TIPF[19], localized to the hub region together with Tkv–mCherry (Fig. 3b), in addition to its reported localization at the hub–GSC interface[19]. Furthermore, Dpp–GFP expressed by hub cells co-localized with Tkv–mCherry expressed in germline (Fig. 3c, *dpp-lexA*^{ts}*>dpp–GFP*, *nos-gal4*^{ts}*>tkv–mCherry*). These results suggest that ligand (Dpp)-receptor (Tkv) engagement and activation occurs at the interface of the MT-nanotube surface and the hub cell plasma membrane. Knockdown of IFT-B components (*oseg2*^{RNAi}, *che-13*^{RNAi} or *osm6*^{RNAi}), which reduces MT-nanotube formation, resulted in reduction of the number of Tkv–GFP puncta in the hub area, concomitant with increased membrane localization of Tkv–GFP (Fig. 3d, f, g). A similar trend was observed upon treatment of the testes with colcemid (Extended Data Fig. 3h, i), suggesting that MT-nanotubes are required for trafficking of Tkv into the hub area. By contrast, knockdown of Klp10A, which causes

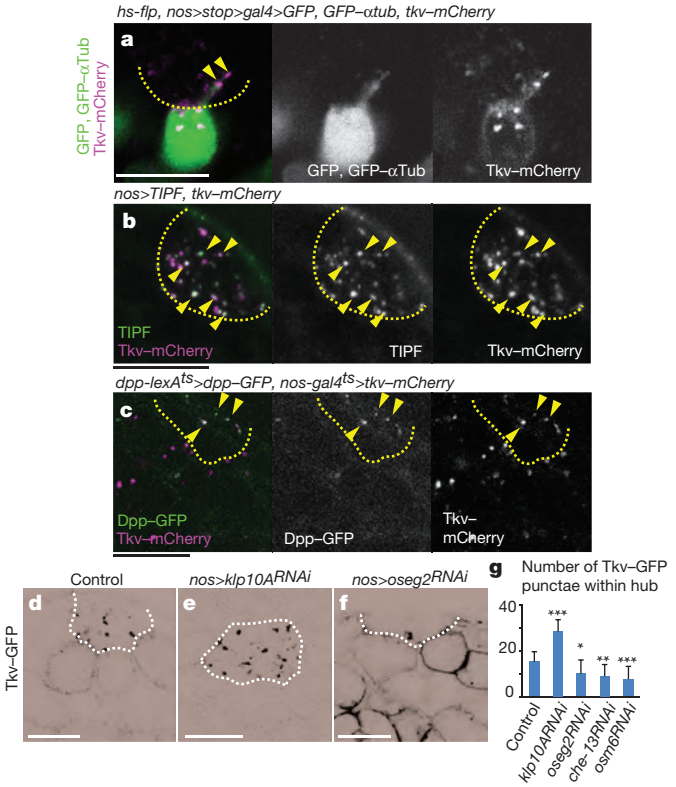

Figure 3 | Dpp signalling components localize to the MT-nanotubes. **a**, A GSC clone expressing Tkv–mCherry, GFP–αTub and GFP (*hs-flp*, *nos-FRT-stop-FRT-gal4*, *UAS–GFP*, *UAS–GFP–αtub*, *UAS-tkv–mCherry*). **b**, An apical tip of the testis expressing TIPF and Tkv–mCherry in germ cells. Arrowheads point to a few of co-localizing puncta. **c**, An apical tip of the testis expressing Dpp in the hub and Tkv in germ cells (*dpp-lexA^{ts}>dpp–GFP*, *nos-gal4^{ts}>tkv–mCherry*). **d**–**f**, Tkv–GFP expressed in control (**d**), *klp10A^{RNAi}* (**e**) and *oseg2^{RNAi}* (**f**) germ cells (*nos-gal4^{ts}>UAS-tkv–GFP*, *UAS-RNAi*). Black and white of micrograph were inverted for better visibility of Tkv localization to the hub and plasma membrane. **g**, Average number and standard deviations of Tkv–GFP puncta within hub area per testis for indicated genotypes. $n = 15$ testes from at least two independent crosses were scored. *P* values from *t*-tests are provided as $*P \leq 0.05$, $**P \leq 0.01$, $***P \leq 0.001$. Scale bar, 10 μm.

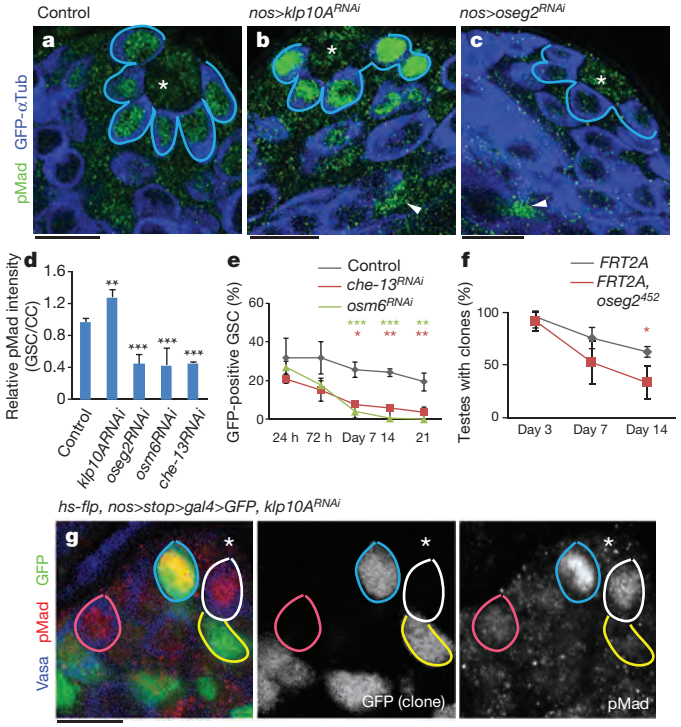

Figure 4 | MT-nanotubes are required for Dpp signalling activation and GSC maintenance. **a**–**c**, pMad staining in control (**a**), *klp10A^{RNAi}* (**b**) and *oseg2^{RNAi}* (**c**) testes. pMad signal in somatic cyst cells (arrowheads), which remains unaffected by germ-cell specific modulation of MT-nanotube components, was used to normalize pMad levels in GSCs. **d**, Quantification of pMad intensity in the GSCs of indicated genotypes. Indicated numbers of GSCs (Extended Data Table 1) from at least two independent crosses were scored for each data point. **e**, **f**, Maintenance of *che-13^{RNAi}*, *osm6^{RNAi}* (**e**) and *oseg2^{452}* (**f**) mutant GSC clones. Indicated numbers of GSCs (Supplementary Table 1) from at least two independent experiments were scored for each data point. **g**, A *klp10A^{RNAi}* GSC clone (72 h after clone induction, blue circle) with a higher pMad level, compared with control GSCs (white circle), *klp10A^{RNAi}* spermatogonia clone (yellow circle) and control spermatogonia clone (pink circle) have similar pMad levels. Asterisk indicates hub. Scale bar, 10 μm. Average value and standard deviations are shown in each graph. *P* values from *t*-tests are provided as $*P \leq 0.05$, $**P \leq 0.01$, $***P \leq 0.001$.

thickening of MT-nanotubes, led to an increase in the number of Tkv–GFP puncta in the hub area (Fig. 3d, e, g). Taken together, these data suggest that Tkv is trafficked into the hub via MT-nanotubes, where it interacts with Dpp secreted from the hub.

Knockdown of *klp10A* (*klp10A^{RNAi}*) led to elevated phosphorylated Mad (pMad) levels, a readout of Dpp pathway activation, in GSCs (Fig. 4a, b, d and Supplementary Note 2). By contrast, RNAi-mediated knockdown of *oseg2*, *osm6* and *che-13* (IFT-B components), which causes shortening of MT-nanotubes, reduced the levels of pMad in GSCs (Fig. 4c, d). Dad-LacZ, another readout of Dpp signalling activation, exhibited clear upregulation upon knockdown of *klp10A* (Extended Data Fig. 4a, b). GSC clones of *che-13^{RNAi}*, *osm6^{RNAi}* or *oseg2^{452}* were lost rapidly compared with control clones (Fig. 4e, f), consistent with the idea that MT-nanotubes help to promote Dpp signal transduction[3,4]. Knockdown of *oseg2*, *che-13* and *osm6* did not visibly affect cytoplasmic microtubules (Extended Data Fig. 4d–g), suggesting that GSC maintenance defects upon knockdown of these genes are probably mediated by their role in MT-nanotube formation. Global RNAi knockdown of these genes in all GSCs using *nos-gal4* did not cause a significant decrease in GSC numbers (data not shown), indicating that compromised Dpp signalling due to MT-nanotube reduction leads to a competitive disadvantage in regards to GSC maintenance only when surrounded by wild-type GSCs.

When *klp10A^{RNAi}* GSC clones were induced, pMad levels specifically increased in those GSC clones, indicating that Klp10A acts cell-autonomously in GSCs to influence Dpp signal transduction (Fig. 4g). Importantly, *klp10A^{RNAi}* spermatogonia (Fig. 4g, yellow line) did not show a significant elevation in pMad level compared with control spermatogonia (Fig. 4.g, pink line), demonstrating that the role of Klp10A in regulation of Dpp pathway is specific to GSCs. pMad levels did not change in spermatogonia upon manipulation of MT-nanotube formation (Extended Data Fig. 4c). GSC clones of *klp10A^{RNAi}* or *klp10A* null mutant (*klp10A^{24}*) did not dominate in the niche, despite upregulation of pMad (Extended Data Fig. 5), possibly because of its known role in mitosis[20]. Importantly, these conditions did not significantly change STAT92E levels, which reflect Upd-JAK-STAT signalling in GSCs[2,21], revealing the selective requirement of MT-nanotubes in Dpp signalling (Extended Data Fig. 6). Together, these results demonstrate that MT-nanotubes specifically promote Dpp signalling and their role in enhancing the Dpp pathway is GSC specific.

Since cytonemes are induced/stabilized by the signalling molecules themselves[18], we explored the possible involvement of Dpp in MT-nanotube formation. First, we found that a temperature-sensitive *dpp* mutant (*dpp^{hr56}/dpp^{hr4}*) exhibited a dramatic decrease in the frequency of MT-nanotubes (0.067 MT-nanotubes per GSC, $n = 244$ GSCs) and the remaining MT-nanotubes were significantly thinner (Fig. 5a, b, Extended Data Fig. 7a, b and Extended Data Table 1). Knockdown of *tkv* (*tkv^{RNAi}*) in GSCs also resulted in reduced length and frequency of MT-nanotubes (Fig. 5a, b, Extended Data Fig. 7c and Extended Data

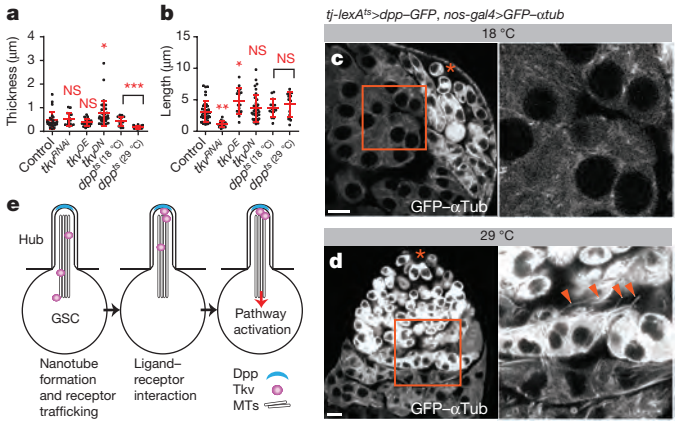

Figure 5 | Dpp signalling is necessary and sufficient for MT-nanotube formation. **a**, **b**, Quantification of MT-nanotube thickness and length in GSCs of indicated genotypes. Each scored value is plotted as a dot. Red line indicates average value and standard deviations. Indicated numbers of nanotubes (Extended Data Table 1) from at least two independent crosses were scored for each genotype. *P* values from *t*-test are provided as $*P \leq 0.05$, $**P \leq 0.01$, $***P \leq 0.001$; NS, non-significant ($P > 0.05$). **c**, **d**, MT-nanotube formation in absence (**c**) or presence (**d**) of Dpp expression in somatic cyst cells. Magnified images of squared regions are shown in right-hand panels. Arrowheads indicate ectopic MT-nanotubes. Asterisk indicates hub. Scale bar, 10 μm. **e**, Model. Dpp induces MT-nanotube formation, and receptor–ligand interaction occurs at the surface of MT-nanotubes, leading to signalling activation in GSCs.

Table 1). Conversely, overexpression of Tkv (tkv^{OE})[22] in germ cells led to significantly longer MT-nanotubes (Fig. 5a, b, Extended Data Fig. 7d and Extended Data Table 1). Interestingly, expression of a dominant negative Tkv (tkv^{DN}), which has intact ligand-binding domain but lacks its intracellular GS domain and kinase domain, resulted in thickening of MT-nanotubes, rather than reducing the thickness/length (Fig. 5a, b and Extended Data Table 1). This indicates that ligand–receptor interaction, but not downstream signalling events, is sufficient to induce MT-nanotube formation. Strikingly, upon ectopic expression of Dpp in somatic cyst cells (*tj-lexA>dpp*), spermatogonia/spermatocytes were observed to have numerous MT-nanotubes (Fig. 5c, d and Extended Data Fig. 7e), suggesting that Dpp is necessary and sufficient to induce or stabilize MT-nanotubes in the neighbouring germ cells. In turn, MT-nanotubes may promote selective ligand–receptor interaction between hub and GSCs, leading to spatially confined self-renewal (Fig. 5e).

Our study shows that previously unrecognized structures, MT-nanotubes, extend into the hub to mediate Dpp signalling. We propose that MT-nanotubes form a specialized cell surface area, where productive ligand–receptor interaction occurs. In this manner, only GSCs can access the source of highest ligand concentration in the niche via MT-nanotubes, whereas gonialblasts do not experience the threshold of signal transduction necessary for self-renewal, contributing to the short-range nature of niche signalling. In summary, the results reported here illuminate a novel mechanism by which the niche specifies stem cell identity in a highly selective manner.

Online Content Methods, along with any additional Extended Data display items and Source Data, are available in the online version of the paper; references unique to these sections appear only in the online paper.

Received 30 October 2014; accepted 1 June 2015.
Published online 1 July 2015.

1. Morrison, S. J. & Spradling, A. C. Stem cells and niches: mechanisms that promote stem cell maintenance throughout life. *Cell* **132,** 598–611 (2008).
2. Tulina, N. & Matunis, E. Control of stem cell self-renewal in *Drosophila* spermatogenesis by JAK-STAT signaling. *Science* **294,** 2546–2549 (2001).
3. Kiger, A. A., Jones, D. L., Schulz, C., Rogers, M. B. & Fuller, M. T. Stem cell self-renewal specified by JAK-STAT activation in response to a support cell cue. *Science* **294,** 2542–2545 (2001).
4. Shivdasani, A. A. & Ingham, P. W. Regulation of stem cell maintenance and transit amplifying cell proliferation by TGF-β signaling in *Drosophila* spermatogenesis. *Curr. Biol.* **13,** 2065–2072 (2003).
5. Kawase, E., Wong, M. D., Ding, B. C. & Xie, T. Gbb/Bmp signaling is essential for maintaining germline stem cells and for repressing bam transcription in the *Drosophila* testis. *Development* **131,** 1365–1375 (2004).
6. Yamashita, Y. M., Jones, D. L. & Fuller, M. T. Orientation of asymmetric stem cell division by the APC tumor suppressor and centrosome. *Science* **301,** 1547–1550 (2003).
7. Davis, D. M. & Sowinski, S. Membrane nanotubes: dynamic long-distance connections between animal cells. *Nature Rev. Mol. Cell Biol.* **9,** 431–436 (2008).
8. Ramírez-Weber, F. A. & Kornberg, T. B. Cytonemes: cellular processes that project to the principal signaling center in *Drosophila* imaginal discs. *Cell* **97,** 599–607 (1999).
9. Avasthi, P. & Marshall, W. F. Stages of ciliogenesis and regulation of ciliary length. *Differentiation* **83,** S30–S42 (2012).
10. Pedersen, L. B. & Rosenbaum, J. L. Intraflagellar transport (IFT) role in ciliary assembly, resorption and signalling. *Curr. Top. Dev. Biol.* **85,** 23–61 (2008).
11. Goetz, S. C. & Anderson, K. V. The primary cilium: a signalling centre during vertebrate development. *Nature Rev. Genet.* **11,** 331–344 (2010).
12. Perrone, C. A. *et al.* A novel dynein light intermediate chain colocalizes with the retrograde motor for intraflagellar transport at sites of axoneme assembly in *Chlamydomonas* and mammalian cells. *Mol. Biol. Cell* **14,** 2041–2056 (2003).
13. Kobayashi, T., Tsang, W. Y., Li, J., Lane, W. & Dynlacht, B. D. Centriolar kinesin Kif24 interacts with CP110 to remodel microtubules and regulate ciliogenesis. *Cell* **145,** 914–925 (2011).
14. Iomini, C., Li, L., Esparza, J. M. & Dutcher, S. K. Retrograde intraflagellar transport mutants identify complex A proteins with multiple genetic interactions in *Chlamydomonas reinhardtii*. *Genetics* **183,** 885–896 (2009).
15. Tran, P. V. *et al.* THM1 negatively modulates mouse sonic hedgehog signal transduction and affects retrograde intraflagellar transport in cilia. *Nature Genet.* **40,** 403–410 (2008).
16. Qin, J., Lin, Y., Norman, R. X., Ko, H. W. & Eggenschwiler, J. T. Intraflagellar transport protein 122 antagonizes Sonic Hedgehog signaling and controls ciliary localization of pathway components. *Proc. Natl Acad. Sci. USA* **108,** 1456–1461 (2011).
17. Cortellino, S. *et al.* Defective ciliogenesis, embryonic lethality and severe impairment of the Sonic Hedgehog pathway caused by inactivation of the mouse complex A intraflagellar transport gene *Ift122/Wdr10*, partially overlapping with the DNA repair gene *Med1/Mbd4*. *Dev. Biol.* **325,** 225–237 (2009).
18. Roy, S., Huang, H., Liu, S. & Kornberg, T. B. Cytoneme-mediated contact-dependent transport of the *Drosophila* decapentaplegic signaling protein. *Science* **343,** 1244624 (2014).
19. Michel, M., Raabe, I., Kupinski, A. P., Perez-Palencia, R. & Bokel, C. Local BMP receptor activation at adherens junctions in the *Drosophila* germline stem cell niche. *Nature Commun.* **2,** 415 (2011).
20. Goshima, G. & Vale, R. D. Cell cycle-dependent dynamics and regulation of mitotic kinesins in *Drosophila* S2 cells. *Mol. Biol. Cell* **16,** 3896–3907 (2005).
21. Schulz, C. *et al.* A misexpression screen reveals effects of bag-of-marbles and TGF beta class signaling on the *Drosophila* male germ-line stem cell lineage. *Genetics* **167,** 707–723 (2004).
22. Dudu, V. *et al.* Postsynaptic Mad signaling at the *Drosophila* neuromuscular junction. *Curr. Biol.* **16,** 625–635 (2006).

Supplementary Information is available in the online version of the paper.

Acknowledgements We thank T. Kornberg, S. Roy, T. Avidor-Reiss, E. Laufer, A. Rodal, D. Sharp, S. Noselli, A. C. Spradling, T. E. Haerry, E. R. Gavis, C.-Y. Lee, T. Xie, B. McCabe, K. S. McKim, Bloomington *Drosophila* Stock Center, Vienna *Drosophila* Resource Center and the Developmental Studies Hybridoma Bank for reagents; S. Roy, T. Kornberg, G. Boekhoff-Falk and D. King for comments and advice; K. Luby-Phelps, A. Bugde and M. Acar for advice for imaging/image data processing; and the Yamashita and Buszczak laboratory members for discussion. The research in the Yamashita laboratory is supported by the Howard Hughes Medical Institute. Y.M.Y. is supported by the MacArthur Foundation.

Author Contributions M.I. conceived the project, and executed experiments. All authors designed experiments, analysed the data, and wrote and edited the manuscript.

Author Information Reprints and permissions information is available at www.nature.com/reprints. The authors declare no competing financial interests. Readers are welcome to comment on the online version of the paper. Correspondence and requests for materials should be addressed to M.B. (michael.buszczak@utsouthwestern.edu) or Y.M.Y. (yukikomy@umich.edu).

METHODS

Fly husbandry and strains. All fly stocks were raised on standard Bloomington medium. The following fly stocks were used: *10XUAS-IVS-myr::GFP* (BDSC32197), *upd-gal4* (BDSC26796), *UAS–GFP–αtub* (BDSC7253 or BDSC7373); *UAS-dpp–GFP* (BDSC53716); *UAS–mCherry* (BDSC35787) and *hs-bam* (BDSC24636) were obtained from Bloomington Stock Center. *UAS-TIPE*[19], *UAS-tkv–GFP, UAS-tkv–mCherry*[18], *dpp-lexA* (LHG)[23], *lexAop-dpp*[23], *UAS-shi*^{ts} (ref. 18), *UAS-dia*^{RNAi} (ref. 18) and *UAS-tkv*^{DN}*2dGSK-3D2* (ref. 18) were gifts from T. Kornberg and S. Roy; *dad-lacZ* (FBti0009617) was a gift from T. Xie; *UAS-tkv–GFP* transgene[22] was a gift from A. Rodal; *tkv–GFP* protein trap line (CPTI-002487) was a gift from B. McCabe; *dpp* loss of function alleles (*dpp*^{hr4} and *dpp*^{hr56})[24,25] were gifts from A. C. Spradling and T. E. Haerry, respectively; *oseg2*^{452}, a null allele of *oseg2*, was a gift from T. Avidor-Reiss[26]; *klp10A*^{24} null clones were generated by FLP/FRT-mediated removal of the rescue transgene in the background of *klp10A* null mutation on the X chromosome: *klp10A*^{24}*/y; klp10A P[acman]BAC (CH322-03M08), 42DFRT/histoneGFP, 42DFRT; hs-flp*-MKRS/TM2; *klp10A*^{24} (FBal0280190) was a gift from K. S. McKim[27]. *P[acman]BAC (CH322-03M08)* transgenic flies were generated using strain BDSC24483 by PhiC31 integrase-mediated transgenesis (BestGene). Flies were heat-shocked at 37 °C for 1 h twice a day for 3 days and dissected after the indicated time.

RNAi screening of candidate genes for MT-nanotube morphology/function was performed by driving *UAS-RNAi* constructs under the control of *nos-gal4* (see below for validation method). Control crosses for RNAi screening were designed with matching *gal4* and UAS copy number using TRiP background stocks (Bloomington Stock Center BDSC36304 or BDSC35787). Expression of Dpp under the *dpp-lexA* (LHG) driver or *tj-lexA* driver (Bloomington Stock Center, BDSC54786) with *tub-gal80*^{ts} (denoted as *dpp-lexA*^{ts} or *tj-lexA*^{ts}, respectively) was performed by culturing flies at 18 °C to avoid lethality during development and shifted to 29 °C upon eclosion for 24 h before analysis. For *shi*^{ts} expression, *nos-gal4>UAS-shi*^{ts} flies cultured at 18 °C were shifted to 29 °C upon eclosion for 24 h before analysis. The *dpp*^{hr56}/CyO; *nos-gal4, UAS–GFP–αtub* females were crossed with *dpp*^{hr4}/SM6 males at permissive temperature (18 °C) and shifted to restrictive temperature (29 °C) upon eclosion for 24 h before analysis. We used *nos-gal4*^{ts} (see below for transgenene construction) to achieve temporal control of *UAS-tkv–mCherry* to obtain similar expression levels to *dpp-lexA*^{ts}*>LexAop-dpp–GFP* for co-localization analysis and quantification of Tkv–GFP puncta. Temperature shift (29 °C) was performed upon eclosion for 72 h before analysis. Expression of *UAS-dome–EGFP*[28] (a gift from S. Noselli) was performed at 18 °C with *nos-gal4* without *VP16* (see below for transgene construction). Other fly crosses were performed at 25 °C. Control experiments were conducted with matching temperature-shift schemes. For clonal expression of Tkv–mCherry and GFP–αTub, *hs-FLP; nos-FRT-stop-FRT-gal4, UAS–GFP*[29] females were crossed with *UAS-tkv–mCherry, UAS–GFP–αtub* males and heat shocked at 37 °C for 20 min and observed 24 h after heat shock. A strong *tkv*^{RNAi} (TRiP.HMS02185, Bloomington Stock Center BDSC40937) led to complete loss of germ cells, while a weak knockdown (TRiP.GL01538, Bloomington Stock Center BDSC43194) partly maintained germ cells and was used for this study. Other stocks used in this study are listed in Extended Data Table 1.

Transgene construction. For constructions of *UAS-dlic–GFP*, *UAS-dlic-VN* and *UAS-klp10A-VN*, open reading flames (ORF) were amplified from whole testis complementary DNA (cDNA) pool using polymerase chain reaction (PCR) with the following primer pairs. For *dlic*: 5′-ctagatctctcaaaatggcgatgaacagtgggacgcaa-3′ and 5′-aactcgagacactcactctgcgacatgtcaattttcacac-3′. These primers amplify BglII-Kozak sequence-*dlic*-XhoI fragment. For *klp10A*: 5′-ctagatctctcaaaatggacatgattac ggtgg-3′ and 5′-aactcgagacgcttgccattcggcgaattg-3′. These primers amplify BglII-Kozak sequence-*klp10A*-XhoI fragment. (BglII and XhoI sites are indicated by underlines.)

Amplified fragments were sequenced for validation and subcloned into BglII/XhoI sites of *pUAST-EGFP–attB*[29] or *pUAST-VenusN-attB* vector (containing the amino (N)-terminal half portion of Venus instead of GFP). *pUAST-VenusN-attB* vector was constructed as follows. The N-terminal half portion of Venus cDNA was amplified using primers, XhoI (underlined)-RSIAT (linker peptide, lower case)-Venus-F; 5′-AACTCGAGagatccattgcgaccATGGTGAGCAAGGGCGA-3′ and KpnI (underlined)-Venus-R; 5′-TCGGTACCTTAGGTGATATAGACGTT GTGGCTGATGTAGT-3′ and subcloned into XhoI/KpnI sites of pUAST-attB vector[30]. Transgenic flies were generated using strain BDSC24749 by PhiC31 integrase-mediated transgenesis (BestGene). *UAS-dlic-VN* and *UAS-klp10A-VN* were used when GFP fluorescence was not necessary or undesirable. *UAS-klp10A*^{RNAi} (double-stranded RNA HMS00920) target sequence is within the 5′ untranslated region (UTR) of the gene and is not present in *UAS-klp10A-VN* construct; thus this transgene was used to rescue RNAi-induced phenotypes (Extended Data Table 1).

To construct *nos-gal4* without *VP16*, Scer\GAL4 cDNA was amplified from the pG4PN-2 vector (a gift from C.-Y. Lee) using the following primers: NdeI (underlined)-*Kozak-gal4* ORF-F: 5′-aagcatatggtcaacatgaagctactgtcttctatc-3′ and EcoRI (underlined)-*gal4* ORF-R: 5′-tactcgaattcttactctttttttgggtttgg-3′. NheI–BamHI flanked the 3.13-kilobase fragment from pCSpnosFGVP (containing the *nanos* 5′ UTR-ATG (NdeI start codon)); the *gal4-VP16-nanos* 3′ UTR (a gift from E. R. Gavis) was subcloned into the NheI–BamHI site of the pUAST-attB vector[30]. NdeI–EcoRI flanking *gal4-VP16* cassette was replaced by the NdeI–EcoRI-digested PCR fragment of Scer\GAL4 cDNA. Transgenes were introduced into the BDSC24482 strain using PhiC31 integrase-mediated transgenesis (BestGene). We used *nos-gal4* without *VP16* in combination with temperature-sensitive *gal80* (*tubulin-gal80*^{ts}), denoted as *nos-gal4*^{ts} to distinguish it from *nos-gal4-VP16* (ref. 31), which has been often referred to as *nos-gal4*.

Live imaging. For visualizing MT-nanotubes in unfixed samples, testes from newly eclosed flies (*nos-gal4>UAS–GFP–αtub*) were dissected in 1 ml of pre-warmed Schneider's *Drosophila* medium supplemented with 10% fetal bovine serum and glutamine–penicillin–streptomycin. Cytochalasin B (10 μM, Sigma-Aldrich) or colcemid (250 μM, Sigma-Aldrich) were added to the media and incubated at room temperature (22–23 °C) for 90 min. Hoechst 33342 (2 μg ml^{-1}) was added as necessary and incubated at room temperature for 30 min. Testes were washed twice with phosphate-buffered saline (PBS) before imaging. For MT-nanotube membrane visualization, testes were dissected in PBS, and FM4-64FX Lipophilic Styryl Dye (5 μg ml^{-1}, Molecular Probes) was added 1 min before analysis. Imaging was performed in the presence of dye within 15 min.

For time-lapse live imaging, testes were placed on a drop of medium on a microscope slide with coverslip spacers on both edges, and another coverslip was placed on top. Time-course images of the areas around hub were taken once every minute or every 5 min for 60 min using a Zeiss LSM700 confocal microscope with a ×40 oil immersion objective (numerical aperture = 1.4). Four-dimensional data sets (*x*, *y*, *z*, *t*) were processed using Image J[32].

Immunofluorescent staining. Testes were dissected in PBS and fixed in 4% formaldehyde in PBS for 30 min. To preserve MT-nanotubes during fixation, taxol (1 μM) was added to 4% formaldehyde/PBS solution. For anti-α-tubulin staining, testes were fixed in 90% methanol, 3% formaldehyde for 10 min at −80 °C. Fixed testes were briefly rinsed three times and permeabilized in PBST (PBS + 0.3% Triton X-100) at room temperature for 1 h, followed by incubation with primary antibody in 3% bovine serum albumin (BSA) in PBST at 4 °C overnight. Samples were washed three times for 20 min in PBST, incubated with secondary antibody in 3% BSA in PBST at room temperature for 2–4 h and then washed for 60 min (three times 20 min) in PBST. Samples were then mounted using VECTASHIELD with 4′,6-diamidino-2-phenylindole (DAPI). The primary antibodies used were as follows: mouse anti-γ-tubulin (1:500; GTU-88, Sigma), rabbit anti-β-galactosidase (1:500, Abcam), rabbit anti-Klp10A (1:2,000, a gift from D. Sharp[33]), rabbit anti-Ser^{453} and Ser^{455} phosphorylated Mad (1:1,000, a gift from E. Laufer), rat anti-Vasa (1:20; developed by A. Spradling and D. Williams), mouse anti-Fasciclin III (7G10, 1:40, developed by C. Goodman), mouse anti-Armadillo (N2 7A1, 1:20, developed by E. Wieschaus) and mouse anti-α-tubulin 4.3 (1:50; developed by C. Walsh) were obtained from the Developmental Studies Hybridoma Bank. Guinea pig anti-STAT92E was generated using the synthetic peptide Ac-CSGTPHHAQESMQLGNGDFGMADFDTITNFENF-amide (Covance) and used at a dilution of 1:2,000. STAT92E antibody was validated by immunofluorescent staining of *nos-gal4*^{ts}*>stat92E*^{RNAi} (Bloomington Stock Center, BDSC35600 and BDSC33637, data not shown). Guinea pig anti-Klp10A was generated as described previously[33] (Covance) and used at a dilution of 1:2,000. AlexaFluor-conjugated secondary antibodies were used at a dilution of 1:400. Images were taken using a Zeiss LSM700 confocal microscope with a ×40 oil immersion objective (numerical aperture = 1.4), or a Leica TCS SP8 confocal microscope with a ×63 oil-immersion objective (numerical aperture = 1.4) and processed using Image J[32] and Adobe Photoshop software. Three-dimensional rendering was performed by Imaris software.

Mosaic analysis and clonal knockdown. The *oseg2*^{452} homozygous clones were generated by FLP/FRT-mediated mitotic recombination[34]. Adult *hs-flp, tub-gal4, UAS–GFP;; tub-gal80, 2AFRT/oseg2*^{452}*, 2AFRT* males were heat-shocked at 37 °C for 1 h twice a day for 3 days; *hs-flp, tub-gal4, UAS–GFP;; tub-gal80, 2AFRT/2AFRT* flies were used as controls. Testes were dissected at indicated times after clone induction. The number of testes containing any GFP-positive *oseg2*^{452} homozygous clones was determined. For RNAi clonal analysis, *hs-flp; nos-FRT-stop-FRT-gal4, UAS–GFP*[29] with *UAS-che-13*^{RNAi}, *UAS-osm6*^{RNAi} or *UAS-klp10A*^{RNAi} flies were heat-shocked at 37 °C for 30 min. Testes were dissected at indicated times after clone induction. The percentage of GFP-positive GSCs was determined. The means ± s.d. from two independent experiments were plotted to the graph.

Quantification of pMad and STAT92E intensities. For pMad quantification, integrated intensity within the GSC nuclear region was measured for anti-pMad staining and divided by the area. To normalize the staining condition, data were further normalized by the average intensities of pMad from four cyst cells in the same testes, and the ratios of relative intensities were calculated as each GSC per average cyst cell. For STAT92E quantification, intensity within the GSC nuclear region was measured for anti-STAT92E staining and divided by the area. Data were normalized by DAPI signal intensities. The means ± s.d. were plotted to the graph for each genotype.

Quantitative reverse transcription PCR to validate RNAi-mediated knockdown of genes. Double driver females (*nos-gal4* and *c587-gal4*) were crossed with males of indicated RNAi lines. Testes from 50 male progenies, age 0–2 days, were collected and homogenized by pipetting in TRIzol Reagent (Invitrogen) and RNA was extracted following the manufacturer's instructions. One microgram of total RNA was reverse transcribed to cDNA using SuperScript III First-Strand Synthesis SuperMix (Invitrogen) with Oligo $(dT)_{20}$ Primer. Quantitative PCR was performed, in triplicate, using Cybergreen Applied Biosystems Gene Expression Master Mix on an CFX96 Real-Time PCR Detection System (Bio-Rad). Control primer for *αtub84B* (5′-TCAGACCTCGAAATCGTAGC-3′/5′-AGCAGTAGAGCTCCCAGCAG-3′) and experimental primer for *oseg1* (5′-TGATCATTCAGCACCTGATCTC-3′/5′-CGCCAGTCGATTCCGATAAA-3′), *oseg2* (5′-TCTGAACGAGCGAGGAAATG-3′/5′-CCACTGGTCATCCTGCTAATC-3′), *oseg3* (5′-ACTGGTTCTCGCAGGTAAAG-3′/5′-TAATGCCTCGCCAAGTGATAG-3′), *osm6* (5′-CTTCCATCCCAAGGAGTGTATC-3′/5′-CTTCTCGTCACTGAAATCGTAGT-3′), *che-13* (5′-GATGGAGCAGGAGCTGAAA-3′/5′-GGTCGGTGGTTTGGTTCT-3′), *tkv* (5′-GCCACGTCTCATCAACTCAA-3′/5′-CTTTGCACCAGCAATGGTAATC-3′) were used. Relative quantification was performed using the comparative CT method (ABI manual).

Statistical analysis and graphing. No statistical methods were used to predetermine sample size. The experiments were not randomized. The investigators were not blinded to allocation during experiments and outcome assessment.

Statistical analysis and graphing were performed using Microsoft Excel 2010 or GraphPad prism 6 software. Data are shown as means ± s.d. The *P* value (two-tailed Student's *t*-test) is provided for comparison with the control shown as $*P \leq 0.05$, $**P \leq 0.01$, $***P \leq 0.001$; NS, non-significant ($P > 0.05$).

MT-nanotube orientation was measured as the angle between the two lines using image]^{32}: one formed by connecting germ cell centre to hub centre; the other formed by connecting the tip and the base of MT-nanotube. Each angle was plotted to Wind Rose graph by Origin 9.1 software (OriginLabs).

23. Yagi, R., Mayer, F. & Basler, K. Refined LexA transactivators and their use in combination with the *Drosophila* Gal4 system. *Proc. Natl Acad. Sci. USA* **107,** 16166–16171 (2010).
24. Wharton, K., Ray, R. P., Findley, S. D., Duncan, H. E. & Gelbart, W. M. Molecular lesions associated with alleles of decapentaplegic identify residues necessary for TGF-β/BMP cell signaling in *Drosophila melanogaster*. *Genetics* **142,** 493–505 (1996).
25. Xie, T. & Spradling, A. C. Decapentaplegic is essential for the maintenance and division of germline stem cells in the *Drosophila* ovary. *Cell* **94,** 251–260 (1998).
26. Avidor-Reiss, T. *et al.* Decoding cilia function. *Cell* **117,** 527–539 (2004).
27. Radford, S. J., Harrison, A. M. & McKim, K. S. Microtubule-depolymerizing kinesin KLP10A restricts the length of the acentrosomal meiotic spindle in *Drosophila* females. *Genetics* **192,** 431–440 (2012).
28. Ghiglione, C. The *Drosophila* cytokine receptor Domeless controls border cell migration and epithelial polarization during oogenesis. *Development* **129,** 5437–5447 (2002).
29. Salzmann, V., Inaba, M., Cheng, J. & Yamashita, Y. M. Lineage tracing quantification reveals symmetric stem cell division in *Drosophila* male germline stem cells. *Cell. Mol. Bioeng.* **6,** 441–448 (2013).
30. Bischof, J., Maeda, R. K., Hediger, M., Karch, F. & Basler, K. An optimized transgenesis system for *Drosophila* using germ-line-specific phiC31 integrases. *Proc. Natl Acad. Sci. USA* **104,** 3312–3317 (2007).
31. Van Doren, M., Williamson, A. L. & Lehmann, R. Regulation of zygotic gene expression in *Drosophila* primordial germ cells. *Curr. Biol.* **8,** 243–246 (1998).
32. ImageJ. (U.S. National Institutes of Health, 1997–2014).
33. Rogers, G. C. *et al.* Two mitotic kinesins cooperate to drive sister chromatid separation during anaphase. *Nature* **427,** 364–370 (2004).
34. Xu, T. & Rubin, G. M. Analysis of genetic mosaics in developing and adult *Drosophila* tissues. *Development* **117,** 1223–1237 (1993).
35. Grieder, N. C., de Cuevas, M. & Spradling, A. C. The fusome organizes the microtubule network during oocyte differentiation in *Drosophila*. *Development* **127,** 4253–4264 (2000).
36. Kuzhandaivel, A., Schultz, S. W., Alkhori, L. & Alenius, M. Cilia-mediated hedgehog signaling in *Drosophila*. *Cell Rep.* **7,** 672–680 (2014).

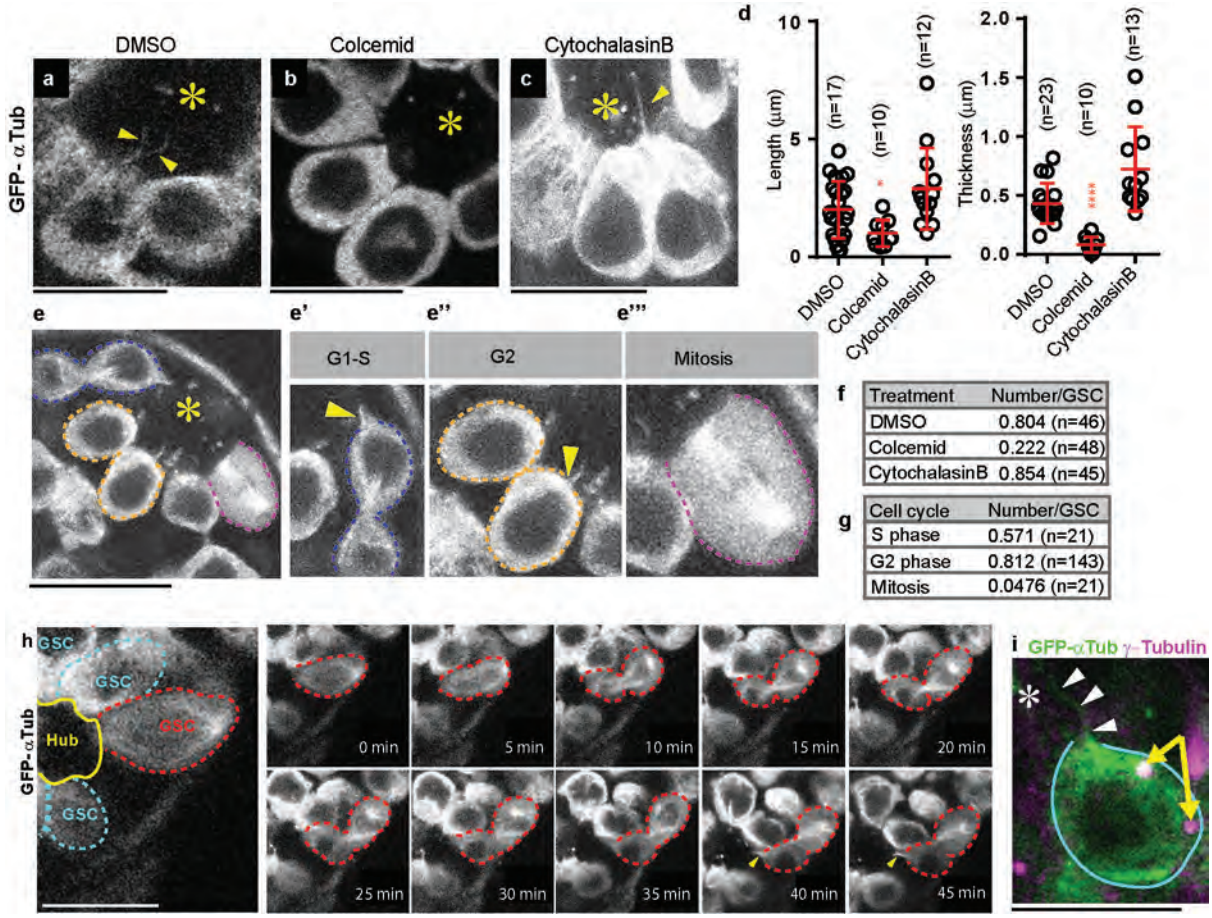

Extended Data Figure 1 | MT-nanotubes are MT-based structures that form in a cell-cycle-dependent manner. **a**–**c**, Representative images of MT-nanotubes visualized by GFP–αTub (*nos-gal4>GFP–αtub*) after 90 min *ex vivo* treatment of mock (**a**, DMSO), colcemid (**b**) or cytochalasin B (**c**). **d**, Thickness and length of MT-nanotubes after mock (DMSO), colcemid or cytochalasin B treatment. Each scored value is plotted as an open circle. Red line indicates average value with standard deviation; *n* indicates the number of MT-nanotubes scored from more than three testes for each data point. **e**, Representative images of MT-nanotubes in each cell cycle stage visualized by GFP–αTub. The three smaller panels to the right show magnified images of GSCs from the larger left-hand panel representing various stages of the cell cycle: left, G1–S phase (before the completion of the cytokinesis); middle, G2 phase; right, mitosis. **f**, **g**, Frequency of MT-nanotubes/GSC after mock (DMSO), colcemid or cytochalasin B treatment (**f**) or during cell cycle (**g**); *n* indicates the number of GSCs scored from more than ten testes from three independent experiments for each data point. **h**, Frames from a time-lapse live imaging of a MT-nanotube visualized by GFP–αTub. GSC in anaphase at 0 min is indicated by the red dotted circle, which undergoes cell division and grows MT-nanotubes (arrowheads) at 40 min (see Supplementary Video 1). MT-nanotubes typically formed during telophase to early S phase of the next cell cycle, within an hour after mitotic entry (95.2%, $n = 21$ GSCs) from three independent experiments. **i**, An example of a GSC that does not have the centrosome (arrows) at the base of the MT-nanotubes. MT-nanotubes are indicated by arrowheads. Centrosomes are indicated by arrows. Asterisk indicates hub. *P* values from *t*-tests are provided as $*P \leq 0.05$, $**P \leq 0.01$, $***P \leq 0.001$. Scale bar, 10 μm.

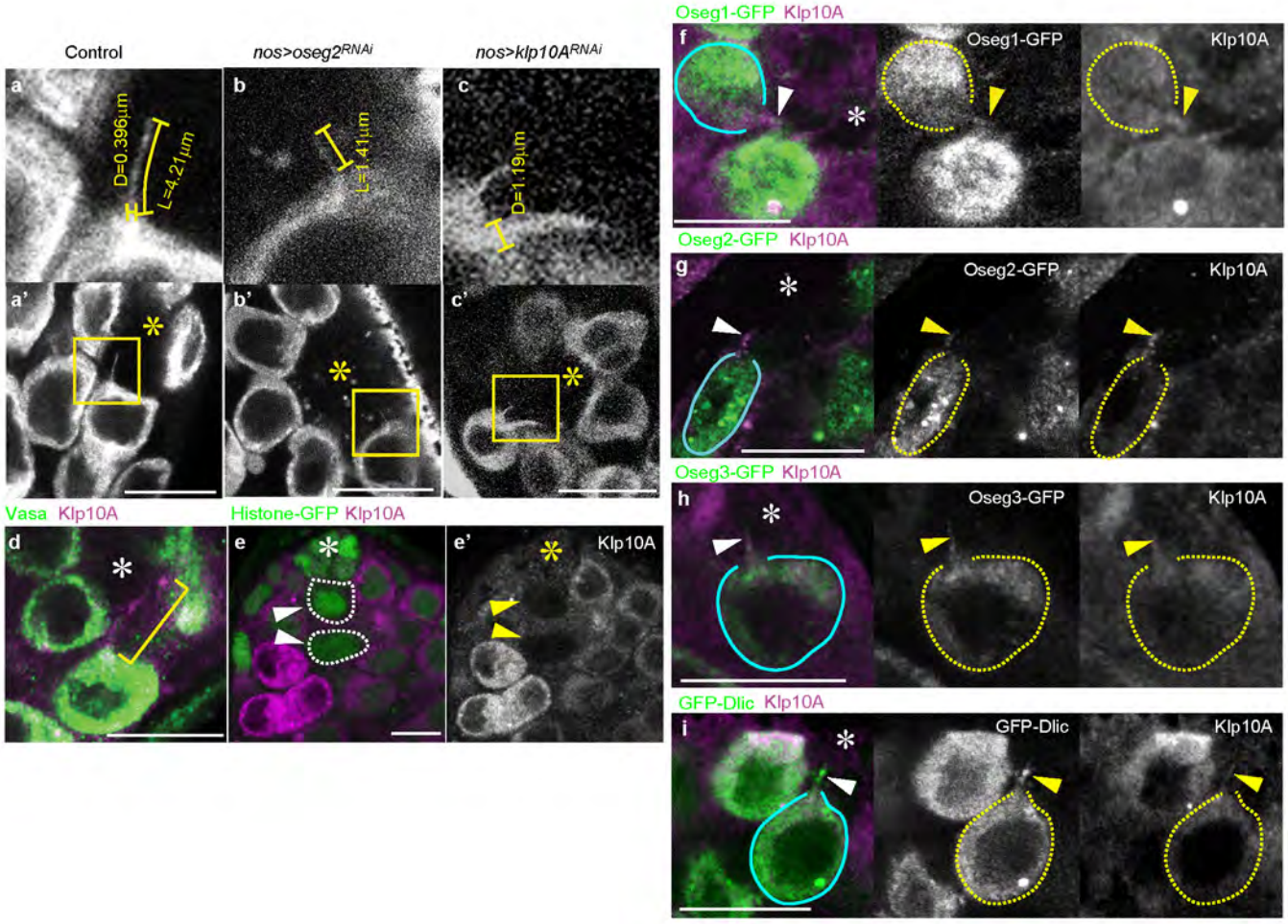

Extended Data Figure 2 | IFT proteins localize to MT-nanotubes. **a**–**c**, Examples of MT-nanotubes in wild type (**a**), *oseg2*^{RNAi} (**b**) and *klp10a*^{RNAi} (**c**) testes; *nos-gal4>GFP–αtub* was used. Upper panels are magnified views of squared areas in lower panels, showing examples of measuring length (*L*) and diameter (*D*, the base of the MT-nanotubes). **d**, An example of a MT-nanotube stained by anti-Klp10A antibody in WT testis. **e**, Validation of anti-Klp10A antibody, showing that *klp10A* mutant clones (arrowheads and dotted circles) have completely lost the staining 3 days after clone induction. **f**–**i**, Examples of testis apical tips expressing Oseg1–GFP (**f**), Oseg2–GFP (**g**), Oseg3–GFP (**h**), GFP–Dlic (**i**) driven by *nos-gal4*. Arrowheads indicate MT-nanotubes illuminated by anti-Klp10A staining. GSCs are indicated by blue lines or yellow dotted circles. Asterisk indicates hub. Scale bar, 10 μm.

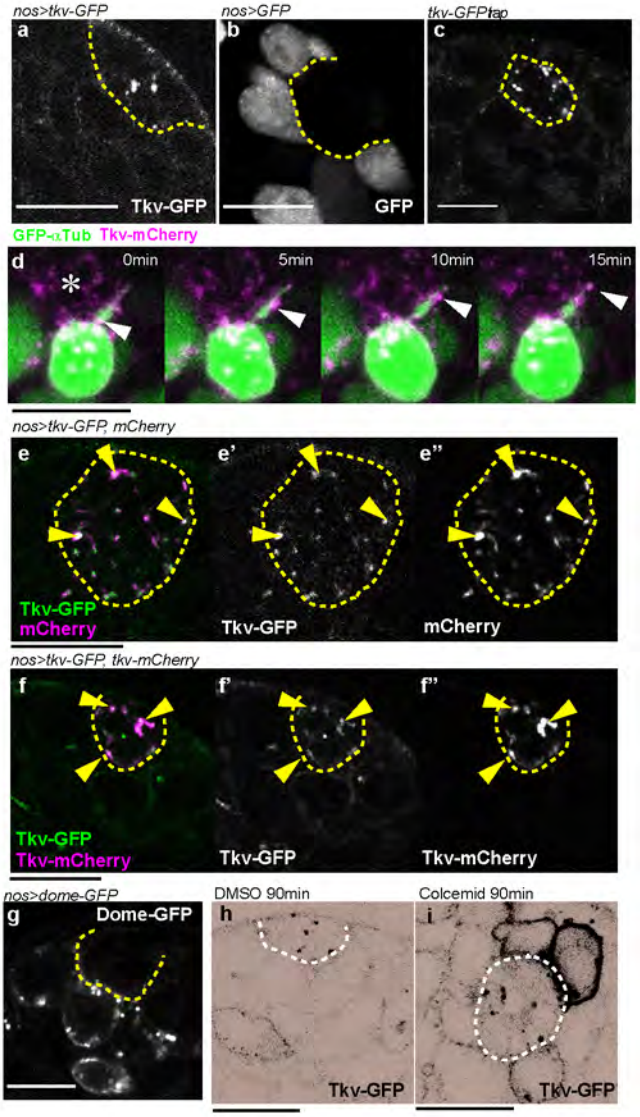

Extended Data Figure 3 | Tkv–mCherry or mCherry co-localize with Tkv–GFP in the hub. **a**, An apical tip of the testis expressing Tkv–GFP in germ cells (*nos-gal4>tkv–GFP*). Broken lines indicate hub. **b**, An apical tip of the testis expressing GFP in germ cells (*nos-gal4>GFP*). **c**, Fully functional Tkv–GFP protein trap shows punctate pattern within the hub area. **d**, Frames from a time-lapse live observation of Tkv–mCherry puncta (arrowheads) moving along a MT-nanotube. Asterisk indicates hub. **e**, mCherry and Tkv–GFP expressed in germ cells (*nos-gal4>UAS-tkv–GFP, UAS–mCherry*) co-localize in the hub (arrowheads). **f**, Tkv–mCherry and Tkv–GFP expressed together in germ cells (*nos-gal4>UAS-tkv–GFP, UAS-tkv–mCherry*) co-localize in the hub (arrowheads). **g**, An apical tip of the testis expressing Dome–GFP in germ cells (*nos-gal4>dome–GFP* raised at 18 °C to reduce the expression level). **h**, **i**, Tkv–GFP localization in control (**h**, DMSO) or colcemid (**i**) treatment, revealing the localization of Tkv–GFP to the GSC cortex upon perturbation of MT-nanotubes. Dotted hemi- or full circles indicate hub. Scale bar, 10 μm.

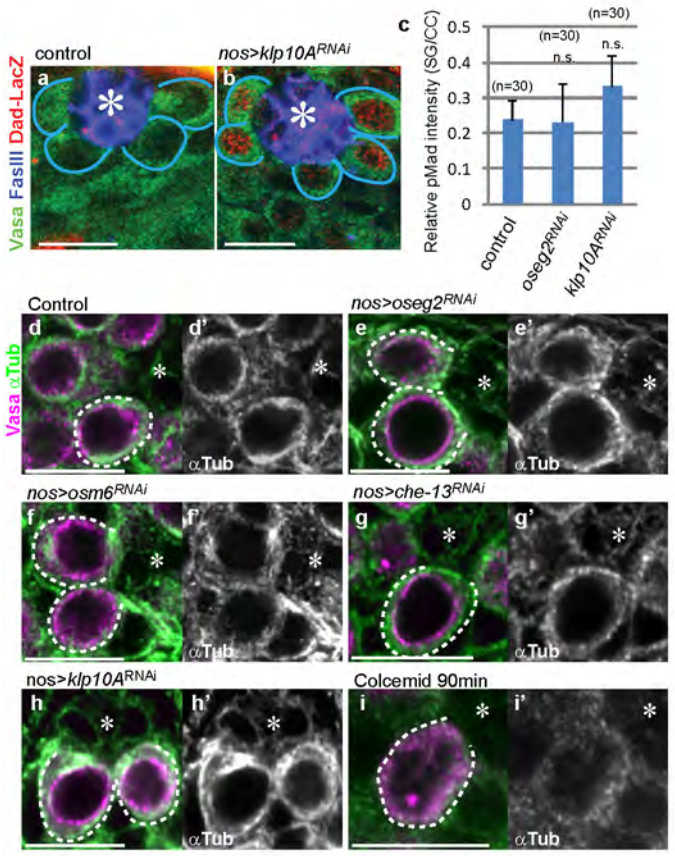

Extended Data Figure 4 | Effect of RNAi-mediated knockdown of IFT components on Dpp signalling and cytoplasmic microtubules. **a**, **b**, Dad-LacZ staining was undetectable in control GSCs (**a**) but was enhanced in *klp10A*^{RNAi} GSCs (**b**). **c**, Quantification of pMad intensity in the two- or four-cell spermatogonia (SG) of indicated genotypes. Graph shows average values ± s.d.; $n = 30$ GSCs were scored from at least ten testes from at least two independent crosses for each data point. **d**–**i**, Cytoplasmic microtubule patterns stained with anti-α-tubulin antibody upon RNAi-mediated knockdown of indicated genes (**d**–**h**) or colcemid treatment for 90 min (**i**). In control as well as upon knockdown of IFT-B components, cytoplasmic MTs, visible as fibrous cytoplasmic patterns, were not visibly affected, whereas colcemid treatment disrupted cytoplasmic MTs; **h**, *klp10A* knockdown led to hyper stabilization of cytoplasmic MTs. Asterisk indicates hub. *P* values from *t*-tests are provided as NS, non-significant ($P > 0.05$). Scale bar, 10 μm.

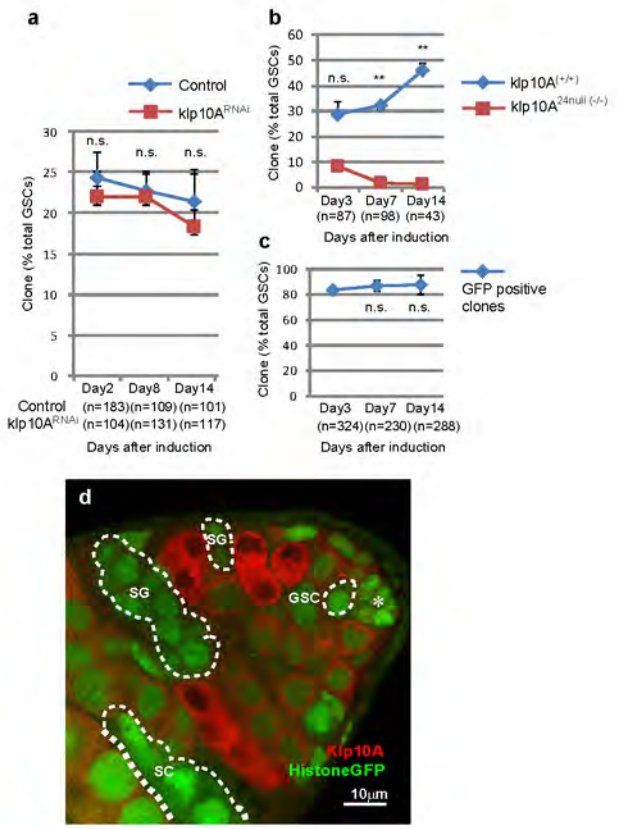

Extended Data Figure 5 | The *klp10A* mutant clones do not show a competitive advantage in GSC maintenance. **a**, Maintenance of *klp10A*^{RNAi} GSC clones. **b**, Maintenance of *klp10A*$^{24\ null}$ clones. The number of control GSC clones (+/+, determined by lack of GFP) and the number of *klp10A*$^{24\ null}$ GSC clones (−/−, determined by anti-Klp10A staining) were scored. **c**, Maintenance of GFP-positive GSC clones from the cross of *42DFRT* X *histoneGFP, 42DFRT; hs-flp*-MKRS/TM2 as a control for *klp10A*$^{24\ null}$ clones in **b**. GFP-positive GSC clones did not decrease compared with day 3, excluding the possibility that *klp10A*$^{24\ null}$ GSC clones were lost because of unrelated mutation(s) on the *histoneGFP, 42DFRT* chromosome. **a**–**c**, Indicated numbers of GSCs were scored for each data point from at least two independent crosses. **d**, A representative image of a testis with *klp10A*$^{24\ null}$ clones. The *klp10A*$^{24\ null}$ germ cells determined by anti-Klp10A staining are encircled by white dotted lines. Asterisk indicates hub. Scale bar, 10 μm. Average values ± s.d. are plotted in graphs. *P* values from *t*-tests are provided as $*P \leq 0.05$, $**P \leq 0.01$, $***P \leq 0.001$; NS, non-significant ($P > 0.05$).

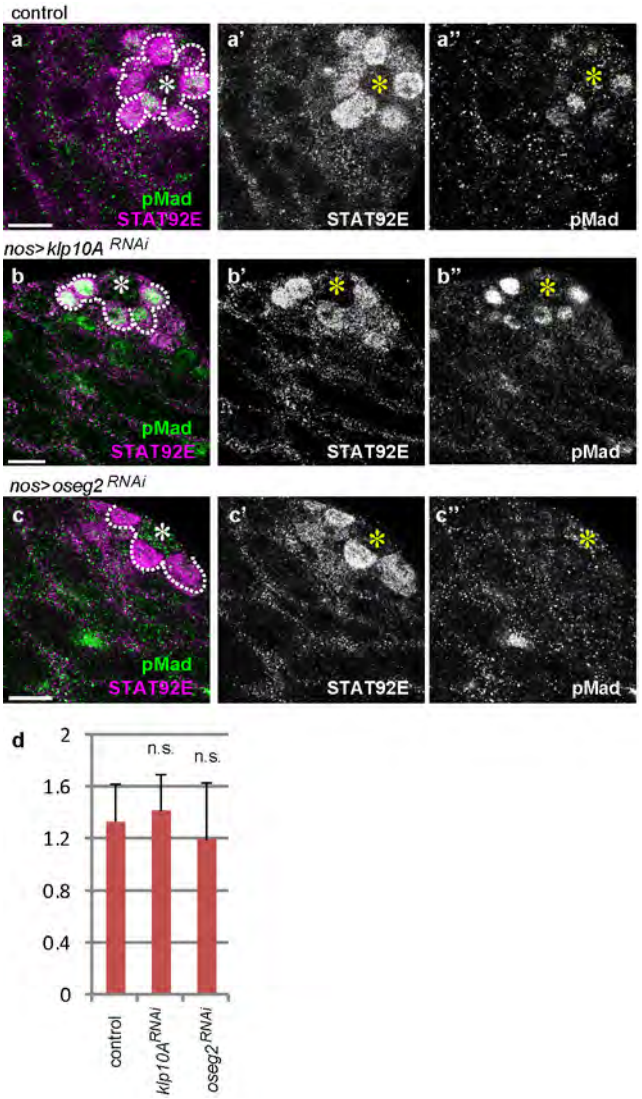

Extended Data Figure 6 | STAT92E level is not affected by modulation of MT-nanotube formation. **a**–**c**, Double staining of STAT92E and pMad in control (**a**), *klp10A*^{RNAi} (**b**) and *oseg2*^{RNAi} (**c**) testes. Asterisk indicates hub. GSCs (and gonialblasts that are still connected to GSCs) are circled by the dotted line. **d**, Quantification of STAT92E intensity. GSCs ($n = 30$) from more than five testes from two independent crosses were scored for each data point. Average values ± s.d. are shown. *P* values from *t*-test are provided as NS, non-significant ($P > 0.05$).

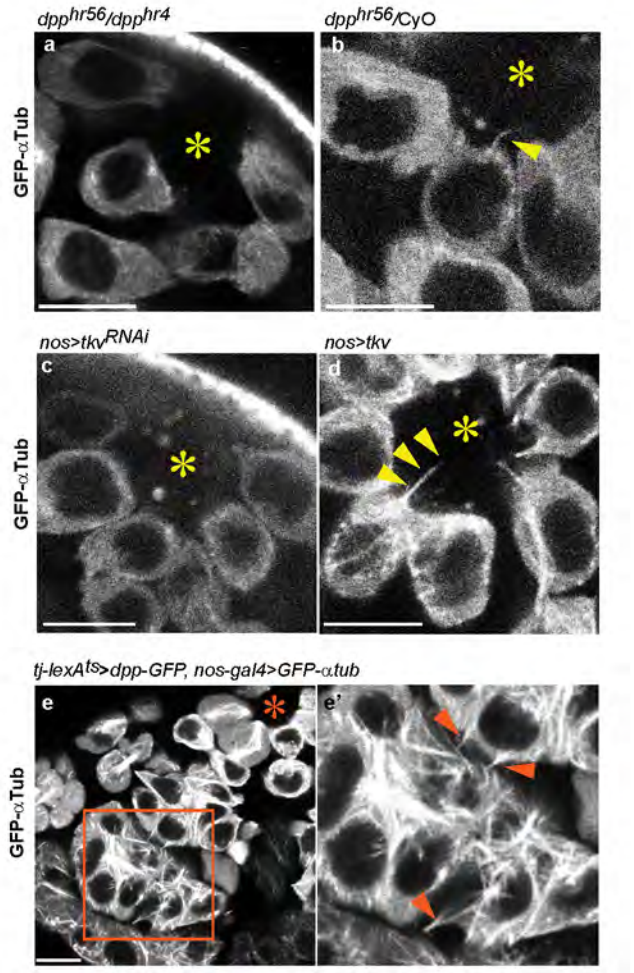

Extended Data Figure 7 | Dpp pathway is required for the MT-nanotube formation. **a**, **b**, Testes (**a**, dpp^{hr56}/dpp^{hr4}) or (**b**, dpp^{hr56}/CyO) expressing GFP–αTub in germ cells (*nos-gal4>GFP–αtub*) at restrictive temperature. **c**, **d**, MT-nanotube formation upon knockdown (**c**) or overexpression (**d**) of Tkv visualized by GFP–αTub. **e**, Ectopic MT-nanotube formation in spermatogonia upon expression of Dpp in somatic cyst cells. The right-hand panel is a magnified view of the squared region in the left panel. Arrowheads indicate ectopic MT-nanotubes. Asterisk indicates hub. Scale bar, 10 μm.

Extended Data Table 1 | Effects of primary cilium or cytoneme genes on MT-nanotube formation

Transgenes	Sources, references	Thickness at the base (μm) ‖ (number of nanotube scored)	Length (μm) † (number of nanotube scored)	MT-nanotube number /GSC (number of GSC scored from n>7 testes)	pMad level GSC/CC †, ‡	RNAi validation
UAS-GFP-αtub§	Bloomington stock center[35]	0.432 (51)	3.32 (82)	0.822 (584)	0.93 (34)	
UAS-Dlic-VN	This study	ND	ND	ND	1.01* (15)	
UAS-Dlic$^{RNAi\ KK107892}$	VDRC	0.412 (17)	1.91* (15)	0.519 (42)↓	0.534*** (15)	
UAS-klp10A-VN	This study	0.398 (39)	2.26* (21)	0.490 (79)↓	0.551*** (15)	
UAS-klp10A$^{RNAi\ TRiP.HMS00920}$	Bloomington stock center	0.827*** (105)	3.7 (65)	0.776 (58)	1.28** (40)	IHC
UAS-klp10A^{RNAi} *with UAS-klp10A-VN*	RNAi rescue‖	0.482 (40)	4.21* (40)	0.960 (75)	0.781(15)	
UAS-oseg1$^{RNAi\ KK101551}$	VDRC	0.569 (16)	3.42 (15)	0.536 (41)	0.722 (15)	qPCR 0.57*
UAS-oseg2$^{RNAi\ GD8122}$	VDRC[36]	0.473 (25)	1.60*** (48)	0.194 (72)↓	0.448*** (44)	qPCR 0.68*
UAS-oseg3$^{RNAi\ KK100864}$	VDRC	0.552 (15)	2.51 (15)	0.663 (66)	0.707 (15)	qPCR 0.19***
UAS-oseg1-GFP	Avidor-Reiss, T[20]	ND	ND	ND	0.832 (15)	
UAS-oseg2-GFP	Avidor-Reiss, T[20]	0.482 (32)	3.99 (309)	0.727 (39)	1.14* (15)	
UAS-oseg3-GFP	Avidor-Reiss, T[20]	0.501 (15)	3.66 (15)	0.750 (37)	0.911 (15)	
UAS-oseg4-GFP	Avidor-Reiss, T[20]	ND	ND	ND	0.701 (15)	
UAS-oseg5-GFP	Avidor-Reiss, T[20]	0.255* (15)	2.62 (15)	0.333 (50) ↓	0.458*** (15)	
UAS-osm6$^{RNAi\ GD24068}$	VDRC	0.477 (15)	2.01* (17)	0.331 (51)↓	0.429*** (15)	qPCR 0.72**
UAS-che-13$^{RNAi\ GD5096}$	VDRC	0.494 (15)	2.16* (33)	0.306 (80)↓	0.449*** (30)	qPCR 0.20***
dpp^{hr56}/*dpp*^{hr4} (29°C 24hr)	Haerry, TE., Spradling, AC[24, 25]	0.173* (20)	4.30 (15)	0.0614 (244)↓	ND	
dpp^{hr56}/*dpp*^{hr4} (18°C)	Haerry, TE, Spradling, AC[24, 25]	0.412 (15)	3.02 (15)	0.545 (33)	ND	
UAS-tkv-GFP	Rodal, A[22]	0.378 (21)	4.89* (15)	0.784 (51)	1.25** (15)	
UAS-tkv$^{DN\ (2d-GSK-3D2)}$	Roy, S[18]	0.779** (34)	3.67 (35)	0.649 (114)	0.679* (15)	
UAS-tkv$^{RNAi\ TRiP.HMS02185}$	Bloomington stock center	0.580 (15)	1.16** (15)	0.234 (90)↓	0.463** (15)	qPCR 0.76*
UAS-caps^{DN}	Roy, S[18]	0.581 (15)	3.71 (15)	0.850 (60)	0.714 (15)	
UAS-dia^{RNAi}	Roy, S[18]	0.407 (15)	3.34 (15)	0.667 (30)	0.991 (15)	
UAS-shi^{ts} (29°C 24hr)	Roy, S[18]	0.536 (15)	3.22 (15)	0.632 (48)	0.894 (15)	
UAS-shi^{ts} (18°C)	Roy, S[18]	0.481 (15)	3.78 (15)	0.701 (44)	0.811 (15)	

UAS-transgenes were driven by *nos-gal4* with *UAS–GFP–αtub*. ND, not determined. For all data points, data were obtained from at least two independent crosses.
† At least 15 randomly selected MT-nanotubes or at least 15 GSCs from more than seven testes were scored.
‡ See Methods for quantification.
§ Control.
‖See Methods for rescue experiment design.
P values from *t*-tests are provided as $*P \le 0.05$, $**P \le 0.01$, $***P \le 0.001$; NS, non-significant ($P > 0.05$). Arrows are based on the significances ($P \le 0.05$). References 35 and 36 are cited in the table.